ACS OMEGA

Open Access

http://pubs.acs.org/journal/acsodf

Article

^{43}Ca MAS-DNP NMR of Frozen Solutions for the Investigation of Calcium Ion Complexation

Tristan Georges, Romain Chèvre, Samuel F. Cousin, Christel Gervais, Pierre Thureau, Giulia Mollica,* and Thierry Azaïs*

Cite This: *ACS Omega* 2024, 9, 4881−4891

Read Online

ACCESS | Metrics & More | Article Recommendations | Supporting Information

ABSTRACT: Calcium ion complexation in aqueous solutions is of paramount importance in biology as it is related to cell signaling, muscle contraction, or biomineralization. However, Ca^{2+}-complexes are dynamic soluble entities challenging to describe at the molecular level. Nuclear magnetic resonance appears as a method of choice to probe Ca^{2+}-complexes. However, ^{43}Ca NMR exhibits severe limitations arising from the low natural abundance coupled to the low gyromagnetic ratio and the quadrupolar nature of ^{43}Ca, which overall make it a very unreceptive nucleus. Here, we show that ^{43}Ca dynamic nuclear polarization (DNP) NMR of ^{43}Ca-labeled frozen solutions is an efficient approach to enhance the NMR receptivity of ^{43}Ca and to obtain structural insights about calcium ions complexed with representative ligands including water molecules, ethylenediaminetetraacetic acid (EDTA), and L-aspartic acid (L-Asp). In these conditions and in combination with numerical simulations and calculations, we show that ^{43}Ca nuclei belonging to Ca^{2+} complexed to the investigated ligands exhibit rather low quadrupolar couplings (with C_Q typically ranging from 0.6 to 1 MHz) due to high symmetrical environments and potential residual dynamics in vitrified solutions at a temperature of 100 K. As a consequence, when ^{1}H→^{43}Ca cross-polarization (CP) is used to observe ^{43}Ca central transition, "high-power" $\nu_{RF}(^{43}Ca)$ conditions, typically used to detect spin 1/2 nuclei, provide ∼120 times larger sensitivity than "low-power" conditions usually employed for detection of quadrupolar nuclei. These "high-power" CPMAS conditions allow two-dimensional (2D) ^{1}H−^{43}Ca HetCor spectra to be readily recorded, highlighting various Ca^{2+}−ligand interactions in solution. This significant increase in ^{43}Ca NMR sensitivity results from the combination of distinct advantages: (i) an efficient ^{1}H-mediated polarization transfer from DNP, resembling the case of low-natural-abundance spin 1/2 nuclei, (ii) a reduced dynamics, allowing the use of CP as a sensitivity enhancement technique, and (iii) the presence of a relatively highly symmetrical Ca environment, which, combined to residual dynamics, leads to the averaging of the quadrupolar interaction and hence to efficient high-power CP conditions. Interestingly, these results indicate that the use of high-power CP conditions is an effective way of selecting symmetrical and/or dynamic ^{43}Ca environments of calcium-containing frozen solution, capable of filtering out more rigid and/or anisotropic ^{43}Ca sites characterized by larger quadrupolar constants. This approach could open the way to the atomic-level investigation of calcium environments in more complex, heterogeneous frozen solutions, such as those encountered at the early stages of calcium phosphate or calcium carbonate biomineralization events.

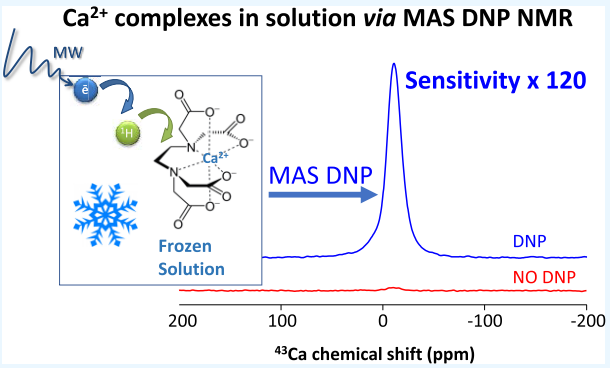

INTRODUCTION

Calcium is the fifth most profuse element in mass in the Earth's crust[1,2] and is of crucial importance for many organisms as it is involved in many physiological processes such as cell signaling,[3,4] muscle contraction,[5] or biomineralization.[6] In both intracellular and extracellular compartiments, spatial and temporal variations of calcium concentrations are controlled by various calcium-binding proteins.[3] On the other hand, excess of calcium ions is suspected to be involved in cardiovascular[7] or neurodegenerative[8] diseases.

Calcium is also used by many organisms to produce mineralized structures or tissues through the precipitation of calcium phosphate or calcium carbonate phases. The biomineralization process is mediated by various specific proteins controlling the nucleation and the crystallization of the final mineral phase through complex mechanisms that remain obscure at the molecular-level conditions for calcium carbonates[9] or bone apatite.[10]

Received: October 26, 2023
Revised: December 11, 2023
Accepted: December 26, 2023
Published: January 19, 2024

As such, calcium−protein complexation is of crucial importance *in vivo*, and its understanding is of paramount importance in various fields of research including biological chemistry, biomineralization, or medicine. However, these calcium-based nanometric soluble entities are challenging to describe at the molecular level. Therefore, nuclear magnetic resonance (NMR) appears as an appealing technique because of its ability to probe dynamics, structure, and interactions at the atomic scale. However, the use of ^{43}Ca NMR is still limited because of severe intrinsic sensitivity drawbacks.[11] Indeed,^{43}Ca, the NMR-active stable isotope of calcium, possesses a natural abundance of only 0.135% and a low gyromagnetic ratio ($|\gamma_{^{43}Ca}|/\gamma_{^{1}H} \sim 0.07$) making it a highly insensitive nucleus. Moreover, ^{43}Ca is a 7/2 quadrupolar spin, that can lead to line broadening effects arising from quadrupolar couplings.[12] Last but not least, in physiological conditions, calcium concentrations are low, around 2.5 mM in vertebrates blood plasma[13−15] and around 10 mM in seawater.[16,17]

Hence, few studies using ^{43}Ca solution NMR are reported on complexed-Ca^{2+} with biomolecules. Dynamical information, such as the exchange rate regime, is mainly extracted from such analyses. When the exchange rate regime is favorable, the complexation site can be determined.[18] For example, Parello et al.[19] correlated ^{43}Ca quadrupole relaxation to a change of the parvalbumin protein conformation during Ca^{2+} complexation. ^{43}Ca solution NMR can also inform on the dynamics of the complex. For example, Andersson *et al.*[20] explored the rigidity of the Ca^{2+}-binding sites in parvalbumin, troponin C, and calmodulin through rotational correlation times analysis.

In the case of solids, ^{43}Ca solid-state NMR is a method of choice to access the Ca^{2+} chemical environment in various classes of materials.[12,21,22] In particular, in solid organic complexes and in metalloproteins, the ^{43}Ca chemical shift was shown to be highly sensitive toward small structural differences within the first coordination sphere of Ca^{2+}, depending on both Ca−O and Ca−N distances, and Ca coordination number,[23,24] hence providing unique insights of the local structure around the Ca site. Moreover, ^{43}Ca solid-state NMR is sensitive to variations of the magnetic shielding and electrical field gradient tensors leading to fine insights into some crystalline structures.[11] However, it is generally admitted that the ^{43}Ca isotropic chemical shift is more sensitive to structural variations than to the quadrupolar parameters. As previously mentioned, applications of ^{43}Ca NMR are rather limited due to the lack of sensitivity at natural abundance, although approaches such as the use of high magnetic field, large rotors, or dedicated signal-enhancing NMR pulse sequences[25−27] allow us to circumvent this issue. The acquisition of one-dimensional (1D) ^{43}Ca spectra is possible within a few hours to a few days leading to the characterization of various synthetic[28−30] and even mineralized biological samples.[31,32] However, getting deeper information from 2D experiments is still impossible at a natural abundance. In this case, it is possible to combine the previously mentioned strategies with ^{43}Ca labeling[33−35] and/or hyperpolarization techniques, such as MAS-DNP.[36]

In MAS-DNP, NMR signal enhancement is achieved by transferring the electronic spin polarization of stable unpaired electrons (usually nitroxides[37]) to the nuclear spins (typically protons) under microwave irradiation at cryogenic temperatures.[38] Following ^{1}H−^{1}H spin diffusion, ^{1}H hyperpolarization is then transferred to the nuclei of interest through a cross-polarization (CP) step, potentially leading to NMR signal enhancements of several orders of magnitude.[39−41] The intensity of the NMR signal under "indirect" (*i.e.* ^{1}H-mediated) DNP depends on the efficiency of spin diffusion among ^{1}H nuclei as well as on the efficiency of cross-polarization. The latter is typically low in the case of a quadrupolar nucleus such as ^{43}Ca because a proper magnetization spin lock, required in CP, can be prevented by the time dependence of the quadrupolar interaction. A viable option to partially circumvent this issue is to use low radio frequency (RF) fields.[42−45] In DNP NMR[36,46−48] applications, RF fields comprised between 0.8 and 20 kHz have been reported on quadrupolar nuclei for proton-to-quadrupolar nucleus CPMAS. In the case of ^{43}Ca, MAS-DNP NMR was successfully used by Lee *et al.*[36] to understand the chemical environment of hydroxyapatite by recording ^{1}H−^{43}Ca dipolar-based 2D correlation spectra that enabled the distinction of core and surface Ca^{2+} sites.

Here, we propose a novel approach to study Ca-based complexes in solution to understand the Ca^{2+} complexation by solute ligands. We show that frozen solutions of Ca-based complexes can be efficiently investigated by using ^{1}H-mediated ^{43}Ca MAS-DNP NMR, enabling molecular-level characterization of the interaction sites around the calcium ions. The MAS-DNP approach benefits from two advantages: (i) the low temperature (100 K) limits the dynamics in solution[49] and allows the use of dipolar-based sequences (such as cross-polarization CP) and (ii) DNP leads to significant ^{43}Ca signal enhancement that enables one to overcome the intrinsic low sensitivity of ^{43}Ca. Different solutions were investigated for which calcium ion is complexed by water molecules, ethylenediaminetetraacetic acid (EDTA), or L-aspartic acid (L-Asp). The latter ligand was chosen to mimic the Ca^{2+} interaction with acidic amino acids commonly found in mineralizing proteins representative of biomineralization processes.

More specifically, our data show that the sensitivity of ^{1}H-mediated ^{43}Ca MAS-DNP NMR experiments carried out on frozen solutions strongly depends on the RF conditions used during ^{1}H→^{43}Ca cross-polarization. In particular, "high-power" ^{43}Ca RF conditions (*i.e.*, typically employed for spin 1/2) exhibit higher performances than "low-power" ^{43}Ca RF conditions (*i.e.*, typically used for quadrupolar nuclei). Using high-power conditions, 2D ^{1}H−^{43}Ca HetCor experiments are readily recorded (30 min to 28 h depending on ^{43}Ca concentration) and can allow us to distinguish calcium complexes when different ligands are present in solution. Importantly, our results suggest that the use of high-power ^{1}H→^{43}Ca CP conditions on frozen solutions provide the required sensitivity to selectively detect highly symmetrical and/or dynamic ^{43}Ca environments and filter out more rigid and/or anisotropic environments, which are not enhanced under these conditions. This approach could open the way to the selective investigation of more complex, heterogeneous calcium-containing solutions as those encountered at early stages of calcium phosphates or calcium carbonate formation in a biomineralization context.

METHODS

Sample Preparation. ^{43}Ca-Labeled $CaCO_3$ (62.2%) was purchased from Cortecnet. All other reagents were purchased from Sigma-Aldrich and used as received.

Calcium Ion Complexed with Water Molecules (Ca−H_2O). The Ca−H_2O sample was prepared by dissolving 6.18 mg of

https://doi.org/10.1021/acsomega.3c08292
ACS Omega 2024, 9, 4881−4891

^{43}Ca-Labeled $CaCO_3$ in 100 μL of HCl aqueous solution (1 M). The solution was degassed with N_2 for 2 h (in order to produce Ca^{2+} acidic aqueous solution free of carbonates) before adding 60 μL of D_2O and 40 μL of glycerol-d_8 (H_2O/D_2O/glycerol-d_8 volume ratio was 5:3:2). Finally, Tris buffer was added (1.22 mg, 50 mM) to raise the pH of the solution to 7. Final Ca^{2+} concentration in the Ca−H_2O sample was 300 mM, and the final H/D molar ratio was around 1:2.

Calcium Ion Complexed with Ethylenediaminetetraacetic Acid (Ca-EDTA-50). The Ca-EDTA-50 sample was prepared similarly to Ca−H_2O with a final Ca^{2+}/EDTA molar ratio fixed to 2:1 (50% EDTA compared to Ca^{2+}). Ethylenediaminetetraacetic acid (EDTA) tetrasodium salt dihydrate $(NaOOCCH_2)_2NCH_2CH_2N(CH_2COONa)_2{\cdot}2H_2O$ was added (3.12 mg, 37.5 mM), the final pH was adjusted to 12 using aqueous NaOH, and the final Ca^{2+} concentration in the Ca-EDTA-50 sample was 75 mM.

Calcium Ion Complexed with L-Aspartic Acid (Ca-LAsp-50 or Ca-LAsp-100). The Ca-LAsp samples were prepared as above except that L-Aspartic acid (0.61 mg, 23 mM) was dissolved into a 46 or 23 mM Ca^{2+} solution, leading to an aspartic acid/Ca^{2+} molar ratio of 1:2 (50% of L-Asp compared to Ca^{2+}; Ca-LAsp-50) or 1:1 (100% of L-Asp compared to Ca^{2+}; Ca-LAsp-100). The final pH of the solutions was about 8.

DNP Samples Preparation. For further DNP characterizations, 1.1 mg (15 mM) of Amupol was dissolved in 100 μL of the desired solution. Then, aliquots of 15 μL of these solutions were placed in 3.2 mm sapphire NMR rotors with Teflon inserts. Rotors were then introduced into the low-temperature DNP probe at 100 K. Solutions were found to be stable with time once the rotors were stored at low temperature (−20 °C) as similar ^{1}H and ^{43}Ca DNP enhancements were obtained after several weeks.

MAS-DNP NMR Experiments. All DNP solid-state NMR spectra were acquired on a Bruker 9.4 T wide-bore magnet with an AVANCE-III-HD NMR console and a 3.2 mm DNP low-temperature double-resonance ^{1}H/^{43}Ca MAS probe (H−Y channel, damped with a 110 pF capacitor on the Y channel). Larmor frequencies were, respectively, 400.13 and 26.93 MHz for ^{1}H and ^{43}Ca. Microwaves were applied using a gyrotron (frequency, 263 GHz; power, 4 W) connected to the NMR probe. All spectra were recorded at a MAS frequency of 8 kHz. ^{1}H MAS spectra were recorded using the Hahn-echo sequence with the echo delay set to one rotor period. The radio frequency (RF) field was 67 kHz for both the 90 and 180° pulses. ^{1}H recycle delays were determined using a saturation recovery scheme and were set to 1.3 × T_1 (typically between 1 and 4 s).

The ^{1}H→^{43}Ca CPMAS experiments were optimized according to two distinct Hartmann−Hahn conditions: (i) a low-power condition ("quadrupolar condition", or "LP CP") where ^{1}H and ^{43}Ca RF fields were set to 11.9 and 0.8 kHz, respectively, and (ii) a high-power condition ("spin 1/2 condition", or "HP CP") where ^{1}H and ^{43}Ca RF fields were set to 56 and 32 kHz, respectively. The ^{1}H→^{43}Ca polarization transfer was achieved through a ramp scheme. The Hartmann−Hahn (HH) profiles for both LP and HP CPMAS conditions are shown in Figure S1. The contact time was found to be optimal at 3 ms in HP CP conditions for Ca−H_2O and Ca-EDTA-50 samples and at 5 ms for Ca-LAsp (Figure S2). CPMAS spectra were recorded with ^{1}H decoupling during acquisition using the spinal-64 scheme (67 kHz). Two-dimensional {^{1}H}^{43}Ca HetCor NMR spectra were obtained using the high-power CP condition and by recording 16 to 2100 scans each and 32−48 t_1 increments. FSLG homonuclear decoupling scheme operating at an effective field of 90 kHz was used for the proton dimension. 1D ^{43}Ca MAS spectra were also recorded using a hyperbolic secant sequence with a hyperbolic secant π-inversion[50] pulse (6.9 kHz, 1000 μs), followed by a 90° selective observation pulse with a recycle delay of 15 s.

Enhancement factors (ε(^{1}H) and ε(^{43}Ca)) were determined by taking the ratio of the ^{1}H and ^{43}Ca signal intensities with and without microwave irradiation, all of the other conditions being identical.

^{43}Ca and ^{1}H chemical shifts were calibrated at 0 ppm based on hydroxyapatite (HA) central transitions (^{43}Ca) and hydroxyl group (^{1}H) at 100 K. More precisely, all of the ^{43}Ca signals of frozen aqueous solutions investigated in this study were referenced to the approximate center of gravity of the ^{43}Ca signal of HA at 9.4 T, which was fixed to 0 ppm (Figures S3 and S4). It must be pointed out that under the experimental conditions employed in this study, chemical shift referencing is not straightforward. Indeed, the standard protocol recommended in the literature[21] relies on the use of 1 M aqueous solution of $CaCl_2$. However, these solutions are solid at 100 K. As a consequence, the low temperature and the change of the physical state from liquid to solid (crystalline or not) might influence the line shape (quadrupolar effects) and the chemical shift of the detected signals. Moreover, the rf circuit properties of the LT CPMAS-DNP probe change significantly when passing from RT to 100 K, which prevents a direct transfer of RT chemical shift calibration to 100 K. Alternative methods for achieving accurate ^{43}Ca chemical shift calibration under cryogenic conditions are currently being explored in our groups and will be the object of a separate study.

Since HA was used for ^{43}Ca chemical shift referencing in this study, the HA ^{43}Ca NMR spectrum was fitted to extract the main line shape parameters. Figure S4 shows the best fit of the LP CP spectrum of HA acquired at 100 K. A good quality fit of the experimental CT line shape was obtained. In particular, two calcium sites (Ca(I) and Ca(II)) are required to correctly reproduce the experimental spectrum, in agreement with previous studies.[36,51] Table S1 shows the best fitting parameters (δ_{iso}(^{43}Ca), C_Q, η_Q), which are in good agreement with corresponding values previously reported on a nanocrystalline HA sample under the same magnetic field and temperature conditions.[36] Hence, our setting matches well the chemical shift referencing used in the work of Lee *et al.*[36] on ^{43}Ca MAS-DNP analysis of a similar sample at the same magnetic field.

^{43}Ca MAS-DNP spectral fitting was carried out using DMFit[52] (spinning sideband manifold) and ssNake[53] (hydroxyapatite central transitions line shape). In particular, the ^{43}Ca spinning side bands manifolds were fitted only including first order quadrupolar contributions, without considering chemical shift anisotropy or dynamic effects.

Numerical Simulations and Calculation of NMR Parameters. Starting from a 13 × 13 × 13 Å^3 box in which a calcium cation Ca^{2+} and two chloride anions Cl^- were initially introduced, 70 H_2O molecules were added and both cell parameters and atomic positions were then relaxed with the Vienna Ab initio Simulation Package (VASP) code[54] based on the Kohn−Sham density functional theory (DFT) and

https://doi.org/10.1021/acsomega.3c08292
ACS Omega 2024, 9, 4881−4891

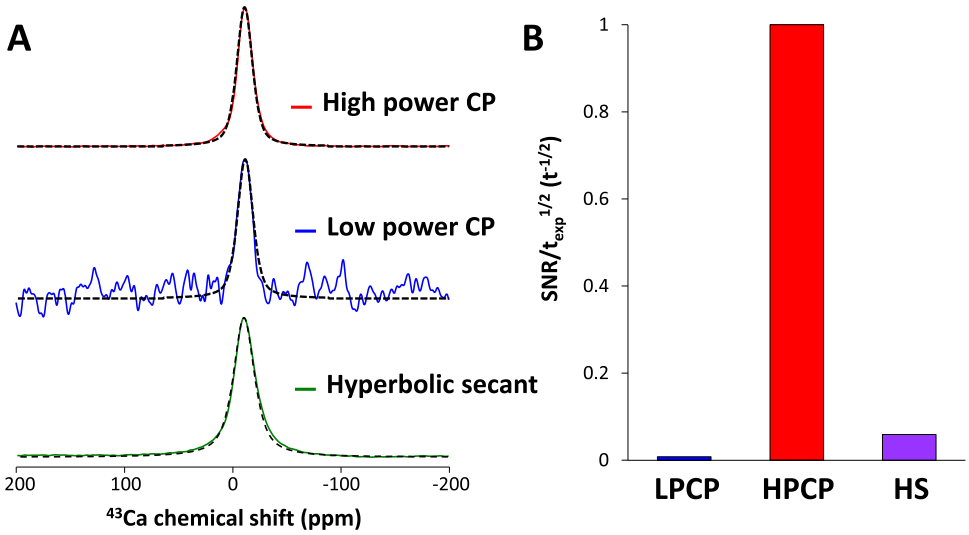

Figure 1. (A) ^{43}Ca MAS-DNP NMR normalized spectra of the Ca−H_2O sample acquired with HP CP (red), LP CP (blue), and HS (green) sequences. Fitting of the central transition is depicted in dashed lines. (B) Normalized sensitivity per unit time constant (see eq (1)) for MAS-DNP NMR spectra of the Ca−H_2O sample acquired in different conditions (all experiments were acquired in the presence of microwave irradiation).

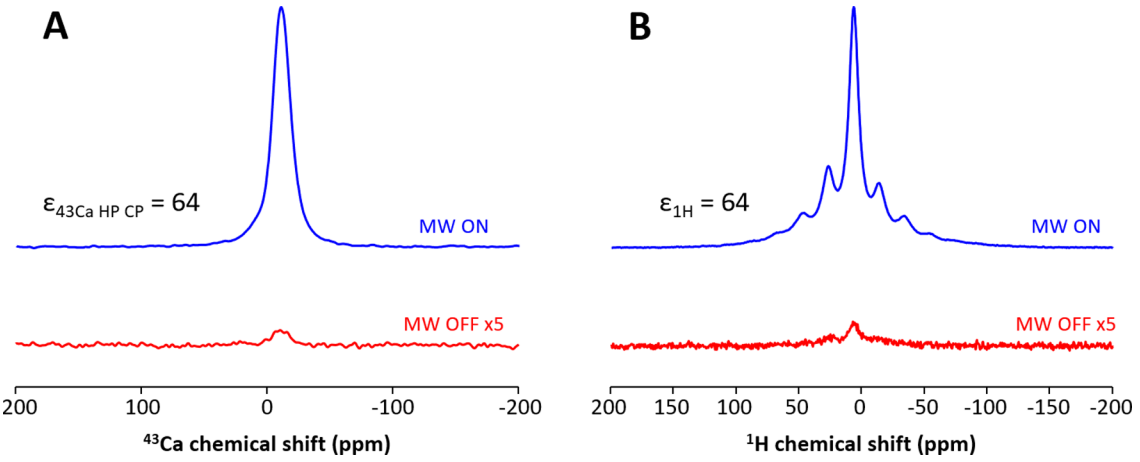

Figure 2. Enhancement factor determination for the Ca−H_2O sample at 100 K by comparison of DNP NMR spectra with (top) and without (bottom) MW. (A) ^{1}H→^{43}Ca HP CPMAS spectra: $\varepsilon_{43CaHPCP}$ = 64. (B) ^{1}H MAS-DNP NMR spectra: ε_{1H} = 64.

using a plane-wave pseudopotential approach. The potential energy surfaces were then explored by *ab initio* molecular dynamics at 300 K with time steps set at 1.5 fs. A microcanonical ensemble in the NVT (constant number of molecules, constant volume, and constant temperature) approach was used. The local energetical minima found were then optimized at 0 K. Similarly, a calcium cation Ca^{2+}, a molecule of ethylenediaminetetraacetate ($EDTA^{4-}$), 62 H_2O molecules, and two H_3O^+ were relaxed in an initial 13 × 13 × 13 Å^3 box. Finally, a calcium cation Ca^{2+}, a molecule of L Aspartate (L-Asp^-), 39 H_2O molecules, and one OH^- were relaxed in an initial 13 × 13 × 13 Å^3 box.

The ^{43}Ca quadrupolar parameters were then calculated on structures optimized at 0 K using the QUANTUM-ESPRESSO code[55] keeping the atomic positions equal to the values previously calculated with VASP. Calculations were performed using the generalized gradient approximation (GGA) with Perdew, Burke, and Ernzerhof (PBE) functionals and norm conserving pseudopotentials[56] in the Kleinman−Bylander form.[57] The wave functions are expanded on a plane-wave basis set with a kinetic energy cutoff of 80 Ry. The experimental value of the quadrupole moment of $^{43}C_Q$ (Q = −40.8 × 10^{-30} m^2) was used to calculate C_Q.[58]

RESULTS AND DISCUSSION

Calcium Ion Complexed with Water Molecules. Figure 1A displays the 1D MAS-DNP NMR spectra of the Ca−H_2O sample obtained under different conditions: ^{1}H→^{43}Ca HP CPMAS, ^{1}H→^{43}Ca LP CPMAS, and direct excitation using the hyperbolic secant (HS) enhancement scheme.[59] Both CP conditions lead to almost identical ^{43}Ca spectra showing a single symmetrical resonance (full width at half-maximum, fwhm = 20.2 ppm) compatible with the presence of Ca^{2+} ions coordinated by water molecules. This similarity between the spectra acquired with the two CP conditions strongly suggests that the ^{43}Ca central transition detected here is not significantly affected by second-order quadrupolar interaction. Interestingly, the HP CPMAS condition is significantly more efficient in terms of sensitivity (SNR = 264 in 4.5 min of acquisition) than the LP CPMAS condition (SNR = 7 in 30 min of acquisition). The comparison of the contact time optimization for Ca−H_2O in low- and high-power CP

https://doi.org/10.1021/acsomega.3c08292
ACS Omega 2024, 9, 4881−4891

conditions (Figure S2) reveals that the $T_{1\rho}$ values for ^{1}H and/or ^{43}Ca are shorter when weak spin-locking fields are used that can explain the difference in CP efficiencies. The absolute efficiency for each condition can be estimated by calculating the sensitivity per unit time (S) as follows:

$$S = \frac{\mathrm{SNR}}{\sqrt{t_{\mathrm{exp}}}} \quad (1)$$

where SNR is the signal-to-noise ratio of a given experiment and t_{exp} is the corresponding experimental time of acquisition. After normalization, the absolute sensitivities of the two ^{1}H→^{43}Ca CPMAS conditions can be compared, revealing that the HP CPMAS condition is ∼120 times more efficient than the LP CPMAS condition for the frozen Ca−H_2O sample (Figure 1B). This highest sensitivity shows that, in our conditions, the ^{43}Ca central transition of the Ca−H_2O sample can be efficiently polarized in CP conditions usually used for spins 1/2 (although I(^{43}Ca) = 7/2). This finding is in line with the absence of a contribution from the second-order quadrupolar interaction to the ^{43}Ca central transition. Combined with ^{43}Ca enrichment, such enhancement could allow the detection of calcium frozen solutions within minutes even at low concentrations (Figure S5).

The high sensitivity generated by the ^{1}H→^{43}Ca HP CP condition allows the acquisition of the HP CPMAS spectrum in the absence of microwave irradiation (MW OFF) — all of the other conditions remaining identical — which enables the determination of the DNP enhancement (ε) for ^{43}Ca as the ratio between the MW ON and the MW OFF HP CPMAS spectra. The DNP enhancement for ^{43}Ca, $\varepsilon_{43\mathrm{CaHPCP}}$ = 64 (Figure 2A), is equivalent to the one obtained for ^{1}H MAS-DNP NMR spectra ($\varepsilon_{1\mathrm{H}}$ = 64; Figure 2B), suggesting a homogeneous distribution of the polarizing agent within the H_2O/D_2O/glycerol-d_8 (5:3:2) frozen solution.

To achieve efficient direct excitation (*i.e.* not *via* ^{1}H nuclei) of quadrupolar and insensitive nuclei like ^{43}Ca, dedicated NMR pulse sequences are typically used, which can significantly increase the sensitivity. Using the HS experiment, the direct-excitation signal of a quadrupolar nucleus can be increased by a theoretical factor of $I \times 2$ (*i.e.*, 7 in the case of ^{43}Ca) by relying on population transfer from satellite transitions to the central transition.[26] The corresponding ^{43}Ca HS NMR (MW ON) spectrum (Figures 1A and S6) is similar to the HP and LP CPMAS spectra. The evaluation of the corresponding absolute efficiency (SNR = 155 in 440 min of acquisition) indicates that the HS experiment is 7 times more efficient than LP CP but 16 times less efficient than HP CP for a Ca−H_2O frozen solution (Figure 1B). We also note that in the presence of residual dynamics and small quadrupolar couplings, the HS scheme is usually less efficient.

The analysis of the spinning sideband manifold of the 1D HP CPMAS-DNP NMR spectrum of Ca−H_2O can be achieved by taking into account the first order quadrupolar interaction, hence allowing the estimation of the C_Q value.[52] The corresponding fitting leads to an average C_Q value ranging from 0.65 to 1.05 MHz (Figure 3). Modeling with a C_Q of 0.65 MHz correctly describes the overall width of the spinning side bands manifold, but the relative intensities of the first side bands are overestimated (Figure 3B). On the other hand, modeling with C_Q = 1.05 MHz leads to a good accuracy for the first four spinning side bands but induces an overestimation of the farthest side bands (Figure 3A). Hence, we cannot exclude

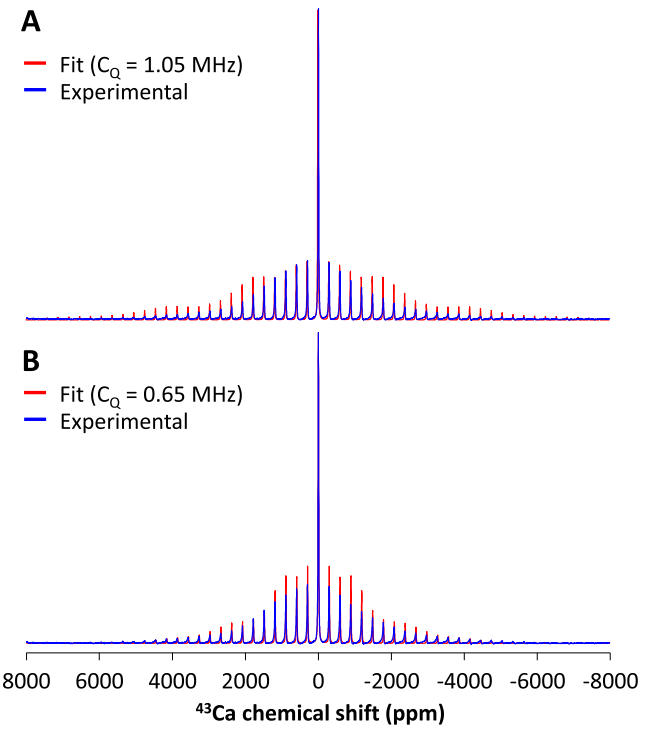

Figure 3. Experimental ^{1}H→^{43}Ca HP CPMAS-DNP NMR spectra (blue) of the Ca−H_2O sample with corresponding fittings (red) using C_Q = 1.05 (A) and 0.65 MHz (B). η_Q was set to 0.75.

that ^{43}Ca irradiation is not large enough for covering the whole spectrum, leading to an underestimation of the farthest side bands. Interestingly, these values are lower than those determined for ^{43}Ca in inorganic crystalline solids (around 1−4 MHz[24]) and agree with the absence of visible second-order quadrupolar line shape for the central transition in our conditions (B_0 = 9.4 T).

Calcium Ion Complexed with Ethylenediaminetetraacetic Acid (EDTA). EDTA is known to be a strong complexing agent for many cations, including Ca^{2+}. In particular, complexation with EDTA occurs in a 1:1 ratio with the metallic cation and it was shown to induce a 6-fold coordination.[60−62] Figure 4A displays the ^{43}Ca DNP NMR spectrum of the Ca-EDTA-50 sample ([EDTA]/[Ca^{2+}] = 1:2) recorded with HP CP conditions. The spectrum exhibits two resonances assigned to Ca^{2+} complexed by water molecules (comparison with the Ca−H_2O sample) and to Ca^{2+} complexed by EDTA at a higher chemical shift. Although, as previously discussed, the exact chemical shift values of the observed ^{43}Ca signals could not be obtained based on standard referencing methods, we note that the two signals corresponding to calcium complexed to EDTA and to H_2O molecules in the frozen solution are separated by 32 ppm, with the Ca-EDTA complex located at higher chemical shift compared to the Ca−H_2O complex. Burgess *et al.* reported two distinct ^{43}Ca signals for crystalline Ca_2(EDTA)·7H_2O corresponding to the two Ca sites at the same magnetic field.[63] These two sites were assigned to calcium fully coordinated by oxygen (Ca I) or to calcium containing two Ca−N bonds (Ca II). The difference in the isotropic chemical shifts of these two Ca sites was 9 ppm. Very interestingly, the relative position of the two sites is in agreement with our data as calcium fully surrounded by oxygens is positioned at a lower chemical shift than calcium complexed by N atoms from EDTA. Hence, coordination to O

https://doi.org/10.1021/acsomega.3c08292
ACS Omega 2024, 9, 4881−4891

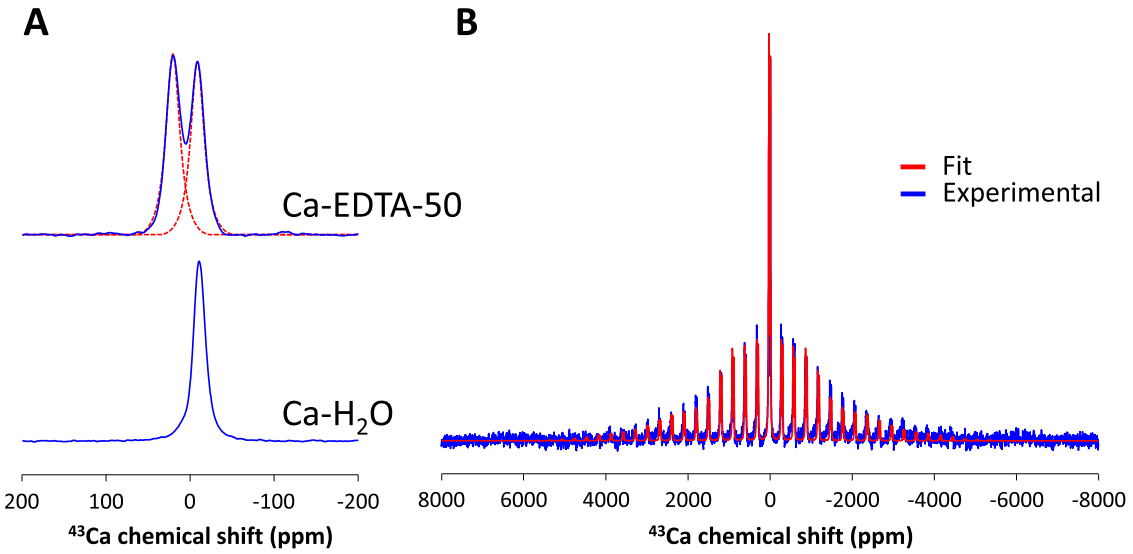

Figure 4. (A) $^{1}H \rightarrow ^{43}Ca$ HP CPMAS-DNP NMR spectrum of Ca-EDTA-50 (top) and Ca−H_2O (bottom) samples. Fitting of the central transition is depicted in red dashed lines. (B) Best fit (red) of the spinning sideband manifold of Ca-EDTA-50 (blue) using two components at 23.7 (Ca^{2+} complexed with EDTA) and −8.5 ppm (Ca^{2+} complexed with water) and C_Q = 0.65 MHz for both. η_Q was set to 0.70 for both components.

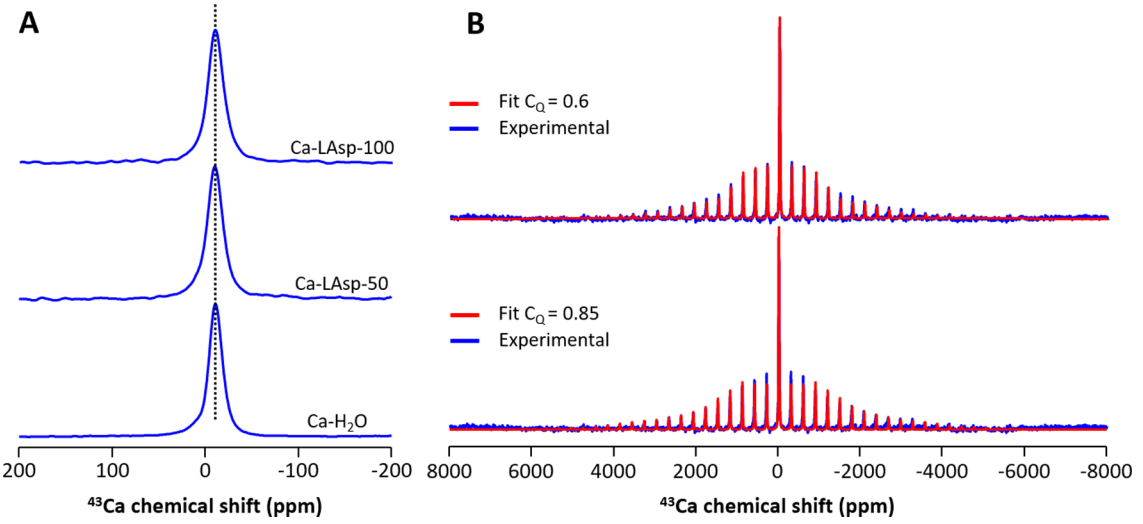

Figure 5. (A) HP CPMAS-DNP NMR spectrum of Ca-LAsp-100 (top), Ca-LAsp-50 (middle), and Ca−H_2O (bottom). (B) Experimental MAS-DNP NMR spectrum of the Ca-LAsp-100 sample (blue) with the corresponding fitting of the spinning sideband manifold (red) using C_Q = 0.6 (top) and 0.85 MHz (bottom).

or N seems to significantly affect the $\delta(^{43}Ca)$ value. Moreover, variations in Ca−N and Ca−O distances in a calcium aminosalicylate model compound were shown to have a strong effect on the ^{43}Ca chemical shift of solid complexes, leading to average chemical shift variations of ∼−30 ppm/Å for Ca−N and Ca−O bonds.[63]

It is important to note that, also in this case, the HP CP condition was found to be more efficient (SNR = 162 within 275 min of acquisition time) than the LP CP condition. Interestingly, both ^{43}Ca signals exhibit 1/1 relative intensities in agreement with the EDTA/Ca^{2+} molar ratio (1:2). Here, if cross-polarization appears to be quantitative, it is probably due to a homogeneous distribution of the polarizing agent in the glassy solution leading to efficient ^{1}H spin diffusion before the $^{1}H \rightarrow ^{43}Ca$ CP transfer. However, we note that the presence of Ca-complexes of high C_Q that would not be detected at our moderate static magnetic field cannot be totally excluded. As in the Ca−H_2O case, it is possible to estimate the C_Q for the Ca-EDTA complex by fitting the spinning sideband manifold with first order quadrupolar coupling. The analysis provides C_Q values of 0.65 ± 0.1 MHz for both Ca^{2+} sites (Figure 4B), slightly lower than the C_Q values estimated for the frozen Ca−H_2O complex and for the solid Ca_2(EDTA)·7H_2O complex determined from a previous study.[63]

Calcium Ion Complexed with L-Aspartic Acid (L-Asp). In order to mimic Ca^{2+} interaction with acidic proteins involved in biomineralization processes, we studied calcium ion complexation with L-Asp, a key amino acid found in large amounts in mineralizing proteins. We investigated two different molar ratios in solution: [L-Asp]/[Ca^{2+}] = 1:2 (Ca-LAsp-50) and 1:1 (Ca-LAsp-100). We have recently shown that in solution, one calcium ion binds with one aspartic acid molecule with a supposed preferential complexation site on the C_1 from aspartic acid.[64] The ^{43}Ca MAS-DNP NMR spectra (HP CP condition) of the three samples (Ca-LAsp-50, Ca-

https://doi.org/10.1021/acsomega.3c08292
ACS Omega 2024, 9, 4881−4891

LAsp-100 and Ca−H_2O) were found to be very similar (Figure 5A) with a ^{43}Ca chemical shift of −9.6 ppm and a line width of 20.2 ppm for Ca-LAsp-50 and Ca-LAsp-100. Only a slight increase of the ^{43}Ca chemical shift (<1 ppm, Figure S7) is observed when Ca^{2+} is complexed to L-Asp when compared to water molecules. Therefore, the complexation to L-Asp does not modify significantly the ^{43}Ca chemical shift of the central transition as already noticed using ^{43}Ca solution NMR,[64] where a variation of 0.1 ppm is observed when passing from 0 to 100% of L-Asp in aqueous solution at pH 7.4. Similarly to the previous samples, Ca-LAsp-50 and Ca-LAsp-100 samples exhibit a symmetrical line shape due to weak quadrupolar coupling. The evaluation of the quadrupolar constant C_Q through the fitting of the spinning side manifold of Ca-LAsp-100 leads to a C_Q value ranging between 0.6 and 0.85 MHz (Figure 5B). We note also that the ^{43}Ca isotropic resonance line width is similar for the three Ca^{2+}-based solute complexes implying that the degree of chemical distribution in the glassy matrix is probably similar.

Numerical Simulations of Calcium Ion Complexation. In order to rationalize the low C_Q values observed and their relationships with chemical environments around Ca^{2+}, we undertook numerical simulations of calcium ion complexation with water, EDTA, and L-Asp (Figures 6 and S8−S11). In the presence of water molecules, Ca^{2+} tends to adopt a 6- to 7-fold coordination (when considering Ca···O distances below 2.7 Å) with an average Ca−OH_2 distance of 2.43 Å (with values ranging from 2.32 to 2.66 Å). Interestingly, the results of our molecular dynamics (MD) simulations agree well with the results of DFT calculations reported by Wong *et al.*,[23] which concluded that 7 water molecules are preferred in the first hydration shell of the Ca^{2+} ions in a dilute $CaCl_2$ solution. Moreover, the range of Ca−O distances predicted by MD is also in agreement with the typical Ca−O distances reported by Wong *et al.* for Ca^{2+} ions coordinated by 6 or 7 water molecules (2.3−2.4 Å). Such arrangements of water ligands lead to C_Q values ranging between 2.17 and 1.34 MHz (Figure S8). If these values are rather small, they are larger than the C_Q average value determined for the Ca−H_2O sample by ^{43}Ca DNP NMR (0.65−1.05 MHz).

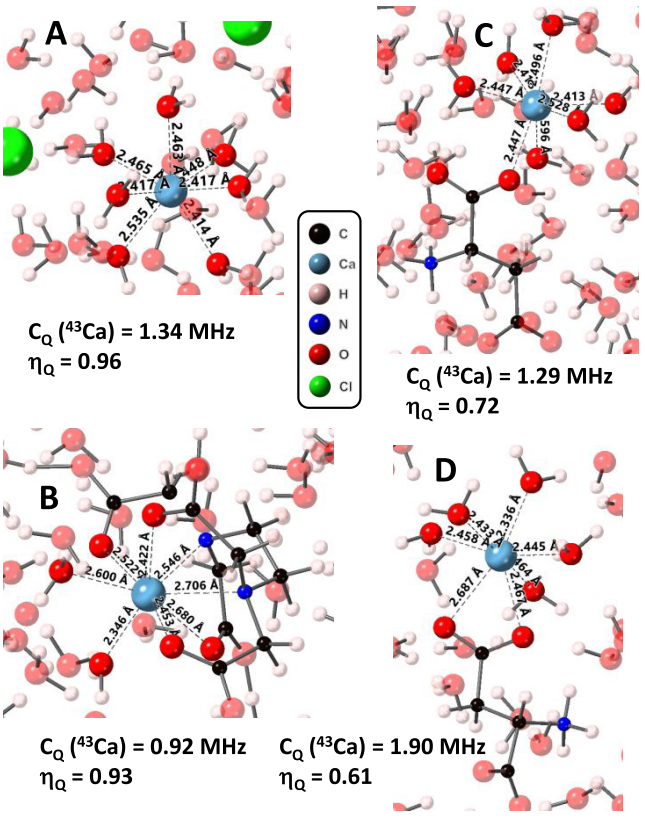

Figure 6. Low-energy configurations obtained by DFT and corresponding calculated ^{43}Ca quadrupolar parameters for (A) Ca^{2+} in interaction with water molecules, (B) Ca^{2+} in interaction with EDTA and water molecules, (C) Ca^{2+} in interaction with L-Asp through C_1OO^-, and (D) Ca^{2+} in interaction with L-Asp through C_4OO^-. Characteristic distances around Ca^{2+} are shown.

In the presence of EDTA, known as a strong complexing agent toward Ca^{2+}, molecular dynamics simulations show that Ca^{2+} tends to adopt a 8-fold coordination through the formation of six coordination bonds with EDTA and two additional water molecules. In this situation, we observe Ca−O distances of 2.35−2.7 Å and Ca−N distances of 2.5−2.7 Å. These distances are in agreement with the values discussed by Burgess *et al.*[63] for similar coordination modes. Such complexation mode is imposing a relatively high symmetrical environment that produces C_Q values ranging between 1.3 and 0.92 MHz (Figure S9). Interestingly, these values, too, are in the same range as those calculated for crystalline Ca_2(EDTA)·$7H_2O$ complexes (∼1 MHz).[63] However, once again, the calculated values are slightly higher than the measured values by ^{43}Ca DNP NMR (0.65 MHz).

Finally, we investigated the complexation by L-Asp that is known to form 1/1 complexes with Ca^{2+}.[64] When considering coordination with the C_1 group, Ca^{2+} tends to adopt a 6- to 7-fold coordination where Ca^{2+} binds to one single oxygen from the C_1OO^- group. The coordination sphere is then completed by 5 to 6 water molecules. It should be noticed that the complexation with 6 water molecules (total coordination of 7) seems more stable and leads to smaller C_Q values of ∼1.29−1.37 MHz (Figure S10). If we consider coordination with the C_4 group, stable Ca^{2+} complexes of similar energies are found. However, the binding mode is slightly different with a bidentate coordination of Ca^{2+} with the C_4OO^- group, the coordination being completed by 4 to 5 water molecules. As observed for the coordination by the C_1 group, the complexation with the maximal coordination (7 with 5 water molecules) looks more stable and leads to smaller C_Q values of ∼1.90−2.42 MHz (Figure S11). Again, calculated values for the two distinct binding modes with L-Asp are higher than the measured values by ^{43}Ca DNP NMR (0.60−0.85 MHz).

The discrepancy between the measured and calculated C_Q values can have two origins. First, an insufficiently large ^{43}Ca irradiation leading to the underestimation of the furthest away spinning side bands intensities leading to the underestimation of C_Q values through the fitting procedure. Second, the presence of residual dynamics at low temperature as some molecular motions[65] or vibrations[66,67] can persist at low temperature leading to a partial averaging of the quadrupolar coupling.

On the basis of these results, different HP and LP CP spectra should be expected depending on the type of calcium environment present in a given sample. Notably, while HP CP conditions should highlight calcium sites characterized by a small "effective" quadrupolar coupling constant (*i.e.*, resulting from relatively symmetric environments and/or the presence of dynamics), the LP CP conditions should also reveal ^{43}Ca

https://doi.org/10.1021/acsomega.3c08292
ACS Omega 2024, 9, 4881−4891

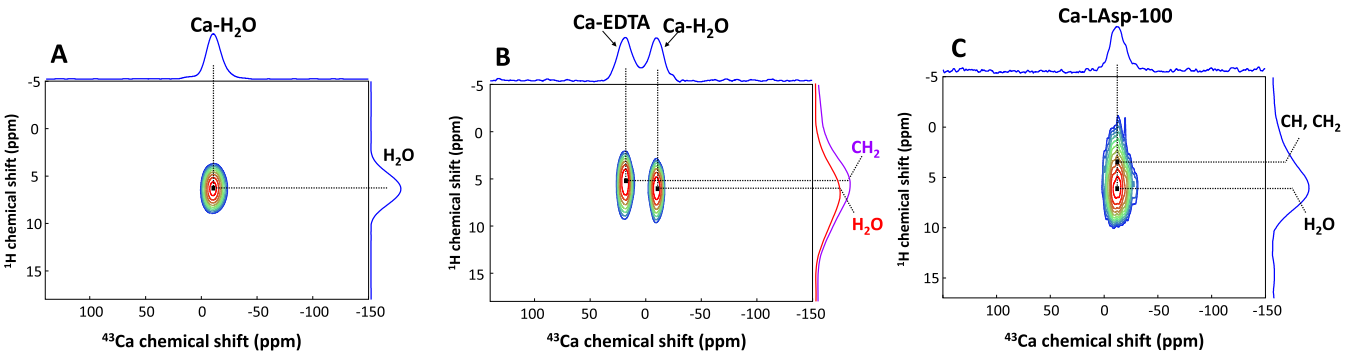

Figure 7. $^{1}H-^{43}Ca$ HetCor spectra of (A) $Ca-H_2O$, (B) Ca-EDTA-50, and (C) Ca-LAsp-100. For Ca-EDTA-50, the two different ^{1}H projections are shown to highlight the distinct protonated environment from Ca^{2+}−water (red line) and Ca^{2+}−EDTA complexes (purple line).

sites that are characterized by larger quadrupolar constants and hence show a correspondingly larger central transition line width. As a striking example, Figure S3 shows that the CPMAS-DNP NMR spectrum of hydroxyapatite powder ($C_Q \approx 2.6$ MHz)[68] acquired using HP "spin 1/2" CP condition resulted in no ^{43}Ca signal (160 scans), while LP "quadrupolar" CP condition provided the ^{43}Ca spectrum of hydroxyapatite central transition (32 scans), hence highlighting the capability of this approach to edit symmetrical and/or dynamic ^{43}Ca environments.

Two-Dimensional $^{1}H-^{43}Ca$ MAS-DNP NMR Experiments. The sensitivity of ^{43}Ca MAS-DNP NMR experiments achieved using the HP CP conditions allowed $^{1}H-^{43}Ca$ heteronuclear correlations (HetCor) experiments to be carried out on the investigated frozen solutions (Figure 7). For the $Ca-H_2O$ solution (Figure 7A), the HetCor experiment shows the presence of a single correlation peak, indicating the presence of an interaction between ^{43}Ca ions and the protons of the coordinated water molecules, identified by a ^{1}H signal of 6.3 ppm. Interestingly, the same experiment performed on the Ca-EDTA-50 solution shows the presence of two distinct correlation peaks (Figure 7B). One peak, very similar to the one observed in the $Ca-H_2O$ sample, indicates the proximity of calcium ions to the coordinated water molecules (^{1}H chemical shift of 6.3 ppm). The second peak reveals an interaction between calcium ions and CH_2 protons of EDTA (^{1}H chemical shift = 5 ppm). Overall, this experiment confirms that water and EDTA both interact with calcium ions in the first coordination sphere. Finally, the Ca-LAsp-100 sample (Figure 7C) exhibits a distorted correlation resonance with a maximum at 6.3 ppm corresponding to water molecules and a shoulder down to 2.5 ppm assigned to CH_2 and CH from L-aspartic acid. Such observation is consistent with the $^{1}H-^{13}C$ MAS-DNP NMR study of $CaCO_3$ formation induced by L-Asp.[64] Thus, two-dimensional $^{1}H-^{43}Ca$ MAS-DNP NMR experiments of vitrified solutions allow the characterization of the spatial proximities between the calcium ion and small ligands for Ca^{2+} complexes.

CONCLUSIONS

^{43}Ca solution NMR is a precious tool to investigate the dynamical aspects of calcium ion complexation mechanisms. However, achieving structural information on Ca-complexes formed in solution using solution NMR remains limited due to the presence of chemical exchange of organic ligands. In this study, we have shown that ^{43}Ca MAS-DNP NMR analysis of frozen solutions can efficiently provide structural insights into calcium ion complexes. In our conditions, Ca^{2+} complexed by water molecules, EDTA, or L-aspartic acid exhibit rather low quadrupolar couplings that can be explained by a highly symmetrical environment combined with the presence of residual dynamics around calcium ion at 100 K. As a consequence, cross-polarization (CP) NMR experiments are much more efficient (~120 more efficient) to detect ^{43}Ca central transition when high-power ν_{RF}(^{43}Ca and ^{1}H) Hartmann−Hahn CP conditions, typically employed to detect spin 1/2 nuclei, are used instead of the low-power conditions, typically used for quadrupolar nuclei. Using high-power CP conditions, and with the help of ^{43}Ca labeling, 2D $^{1}H-^{43}Ca$ HetCor spectra can be readily recorded, highlighting the different Ca^{2+}−ligand interactions in solutions. This approach holds promise to study more complex interactions such as Ca^{2+} with macromolecules or proteins to understand biological functions related to calcium complexation. Moreover, other complexes in solution could be studied by this approach that combines distinct advantages in terms of sensitivity: (i) significant enhancement from DNP, (ii) reduced dynamics allowing the use of CP as a sensitivity enhancement technique, and (iii) relatively high symmetrical environment combined to residual dynamics leading to the averaging of the quadrupolar interaction and thus leading to efficient high-power CP conditions. Importantly, using high-power CP conditions seems to be an effective way of editing ^{43}Ca environments characterized by small "effective" quadrupolar coupling constants (*i.e.*, resulting from relatively symmetric environments and/or the presence of dynamics) while filtering out more rigid and/or anisotropic ^{43}Ca sites characterized by larger quadrupolar constants, for which these conditions are unable to provide efficient cross-polarization transfer.

ASSOCIATED CONTENT

Supporting Information

The Supporting Information is available free of charge at https://pubs.acs.org/doi/10.1021/acsomega.3c08292.

Additional ^{1}H and ^{43}Ca MAS-DNP NMR spectra and additional low-energy configurations of the investigated complexes obtained by DFT calculations (PDF)

AUTHOR INFORMATION

Corresponding Authors

Giulia Mollica − *Aix Marseille Univ, CNRS, ICR, 13397 Marseille, France;* orcid.org/0000-0002-6896-2447; Email: giulia.mollica@univ-amu.fr

https://doi.org/10.1021/acsomega.3c08292
ACS Omega 2024, 9, 4881−4891

Thierry Azaïs − *Sorbonne Université, CNRS, Laboratoire de Chimie de la Matière Condensée de Paris (LCMCP), 75005 Paris, France;* orcid.org/0000-0002-9031-872X; Email: thierry.azais@sorbonne-universite.fr

Authors

Tristan Georges − *Sorbonne Université, CNRS, Laboratoire de Chimie de la Matière Condensée de Paris (LCMCP), 75005 Paris, France*

Romain Chèvre − *Aix Marseille Univ, CNRS, ICR, 13397 Marseille, France*

Samuel F. Cousin − *Aix Marseille Univ, CNRS, ICR, 13397 Marseille, France;* orcid.org/0000-0002-7021-478X

Christel Gervais − *Sorbonne Université, CNRS, Laboratoire de Chimie de la Matière Condensée de Paris (LCMCP), 75005 Paris, France*

Pierre Thureau − *Aix Marseille Univ, CNRS, ICR, 13397 Marseille, France;* orcid.org/0000-0002-9157-256X

Complete contact information is available at: https://pubs.acs.org/10.1021/acsomega.3c08292

Notes

The authors declare no competing financial interest.

■ ACKNOWLEDGMENTS

T.A. and T.G. acknowledge NTU-CNRS "Excellence Science" Joint Research Program for funding. Theoretical calculations were performed using HPC resources from GENCI-IDRIS (Grant 097535). G.M. acknowledges funding from the European Research Council (ERC) under the European Union Horizon 2020 research and innovation programme (Grant Agreement No. 758498).

■ REFERENCES

(1) Anderson, J. S. Chemistry on the Earth. *J. Proc. R. Soc. N.S.W.* **1943**, *76* (30), 329−344.
(2) Fleischer, M. The Abundance and Distribution of the Chemical Elements in the Earth's Crust. *J. Chem. Educ.* **1954**, *31* (9), No. 446.
(3) Sanders, D.; Brownlee, C.; Harper, J. F. Communicating with Calcium. *Plant Cell* **1999**, *11* (4), 691−706.
(4) Ma, X.; Warnier, M.; Raynard, C.; Ferrand, M.; Kirsh, O.; Defossez, P.-A.; Martin, N.; Bernard, D. The Nuclear Receptor RXRA Controls Cellular Senescence by Regulating Calcium Signaling. *Aging Cell* **2018**, *17* (6), No. e12831.
(5) Kuo, I. Y.; Ehrlich, B. E. Signaling in Muscle Contraction. *Cold Spring Harb. Perspect. Biol.* **2015**, *7* (2), No. a006023.
(6) Kahil, K.; Weiner, S.; Addadi, L.; Gal, A. Ion Pathways in Biomineralization: Perspectives on Uptake, Transport, and Deposition of Calcium, Carbonate, and Phosphate. *J. Am. Chem. Soc.* **2021**, *143* (50), 21100−21112.
(7) Reid, I. R.; Birstow, S. M.; Bolland, M. J. Calcium and Cardiovascular Disease. *Endocrinol. Metab.* **2017**, *32* (3), 339−349.
(8) Mattson, M. P. Calcium and Neurodegeneration. *Aging Cell* **2007**, *6* (3), 337−350.
(9) Marin, F.; Luquet, G. Unusually Acidic Proteins in Biomineralization. In *Handbook of Biomineralization*; John Wiley & Sons, Ltd, 2007; pp 273−290.
(10) Boskey, A. L.; Villarreal-Ramirez, E. Intrinsically Disordered Proteins and Biomineralization. *Matrix Biol.* **2016**, *52*−*54*, 43−59.
(11) Leroy, C.; Bryce, D. L. Recent Advances in Solid-State Nuclear Magnetic Resonance Spectroscopy of Exotic Nuclei. *Prog. Nucl. Magn. Reson. Spectrosc.* **2018**, *109*, 160−199.
(12) Bryce, D. L. Calcium Binding Environments Probed by (43)Ca NMR Spectroscopy. *Dalton Trans.* **2010**, *39* (37), 8593−8602.
(13) Cole, W. H. Comparative Animal Physiology. C. Ladd Prosser, Ed. Philadelphia: Saunders, 1950. 888 Pp. $12.50. *Science* **1951**, *113* (2938), 456−457.
(14) Kokubo, T.; Takadama, H. How Useful Is SBF in Predicting in Vivo Bone Bioactivity? *Biomaterials* **2006**, *27*, 2907−2915.
(15) Bold, A. M. Determination of Calcium in Plasma; A Review of Some Modern Methods. *Ann. Clin. Biochem.: Int. J. Lab. Med.* **1970**, *7* (5), 131−135.
(16) Culkin, F.; Cox, R. A. Sodium, Potassium, Magnesium, Calcium and Strontium in Sea Water. *Deep Sea Res. Oceanogr. Abstr.* **1966**, *13* (5), 789−804.
(17) Thompson, M. E.; Ross, J. W. Calcium in Sea Water by Electrode Measurement. *Science* **1966**, *154* (3757), 1643−1644.
(18) Becker, W.; Bhattiprolu, K. C.; Gubensäk, N.; Zangger, K. Investigating Protein−Ligand Interactions by Solution Nuclear Magnetic Resonance Spectroscopy. *ChemPhysChem* **2018**, *19* (8), 895−906.
(19) Parello, J.; Lilja, H.; Cave, A.; Lindman, B. A 43Ca NMR Study of the Binding of Calcium to Parvalbumins. *FEBS Lett.* **1978**, *87* (2), 191−195.
(20) Andersson, T.; Drakenberg, T.; Forsen, S.; Thulin, E.; Swaerd, M. Direct Observation of the Calcium-43 NMR Signals from Calcium(2+) Bound to Proteins. *J. Am. Chem. Soc.* **1982**, *104* (2), 576−580.
(21) Laurencin, D.; Smith, M. E. Development of (43)Ca Solid State NMR Spectroscopy as a Probe of Local Structure in Inorganic and Molecular Materials. *Prog. Nucl. Magn. Reson. Spectrosc.* **2013**, *68*, 1−40.
(22) Widdifield, C. M. Applications of Solid-State 43Ca Nuclear Magnetic Resonance: Superconductors, Glasses, Biomaterials, and NMR Crystallography. In *Annual Reports on NMR Spectroscopy*; Webb, G. A., Ed.; Academic Press, 2017; Chapter 5, Vol. *92*, pp 227−363.
(23) Wong, A.; Laurencin, D.; Wu, G.; Dupree, R.; Smith, M. E. An Ab Initio Quantum Chemical Investigation of 43Ca NMR Interaction Parameters for the Ca2+ Sites in Organic Complexes and in Metalloproteins. *J. Phys. Chem. A* **2008**, *112* (40), 9807−9813.
(24) Gervais, C.; Laurencin, D.; Wong, A.; Pourpoint, F.; Labram, J.; Woodward, B.; Howes, A. P.; Pike, K. J.; Dupree, R.; Mauri, F.; Bonhomme, C.; Smith, M. E. New Perspectives on Calcium Environments in Inorganic Materials Containing Calcium−Oxygen Bonds: A Combined Computational−Experimental 43Ca NMR Approach. *Chem. Phys. Lett.* **2008**, *464* (1), 42−48.
(25) Kentgens, A. P. M.; Verhagen, R. Advantages of Double Frequency Sweeps in Static, MAS and MQMAS NMR of Spin I = 3/2 Nuclei. *Chem. Phys. Lett.* **1999**, *300* (3), 435−443.
(26) Siegel, R.; Nakashima, T. T.; Wasylishen, R. E. Sensitivity Enhancement of MQMAS NMR Spectra of Spin 3/2 Nuclei Using Hyperbolic Secant Pulses. *Chem. Phys. Lett.* **2005**, *403* (4−6), 353−358.
(27) Burgess, K. M. N.; Perras, F. A.; Moudrakovski, I. L.; Xu, Y.; Bryce, D. L. High Sensitivity and Resolution in 43Ca Solid-State NMR Experiments. *Can. J. Chem.* **2015**, *93* (8), 799−807.
(28) Laurencin, D.; Li, Y.; Duer, M. J.; Iuga, D.; Gervais, C.; Bonhomme, C. A 43 Ca Nuclear Magnetic Resonance Perspective on Octacalcium Phosphate and Its Hybrid Derivatives. *Magn. Reson. Chem.* **2021**, *59* (9−10), 1048−1061.
(29) Bonhomme, C.; Wang, X.; Hung, I.; Gan, Z.; Gervais, C.; Sassoye, C.; Rimsza, J.; Du, J.; Smith, M. E.; Hanna, J. V.; Sarda, S.; Gras, P.; Combes, C.; Laurencin, D. Pushing the Limits of Sensitivity and Resolution for Natural Abundance 43Ca NMR Using Ultra-High Magnetic Field (35.2 T). *Chem. Commun.* **2018**, *54* (69), 9591−9594.
(30) Singer, J. W.; Yazaydin, A. Ö.; Kirkpatrick, R. J.; Bowers, G. M. Structure and Transformation of Amorphous Calcium Carbonate: A Solid-State 43Ca NMR and Computational Molecular Dynamics Investigation. *Chem. Mater.* **2012**, *24* (10), 1828−1836.
(31) Ajili, W.; Laurent, G.; Menguy, N.; Gansmuller, A.; Huchette, S.; Auzoux-Bordenave, S.; Nassif, N.; Azaïs, T. Chemical Heterogeneities within the Disordered Mineral Domains of Aragonite

Platelets in Nacre from the European Abalone Haliotis Tuberculata. *J. Phys. Chem. C* **2020**, *124* (26), 14118−14130.
(32) Xu, J.; Zhu, P.; Gan, Z.; Sahar, N.; Tecklenburg, M.; Morris, M. D.; Kohn, D. H.; Ramamoorthy, A. Natural-Abundance 43Ca Solid-State NMR Spectroscopy of Bone. *J. Am. Chem. Soc.* **2010**, *132* (33), 11504−11509.
(33) Wong, A.; Laurencin, D.; Dupree, R.; Smith, M. E. Two-Dimensional 43Ca−1H Correlation Solid-State NMR Spectroscopy. *Solid State Nucl. Magn. Reson.* **2009**, *35* (1), 32−36.
(34) Wang, Y.; Von Euw, S.; Fernandes, F. M.; Cassaignon, S.; Selmane, M.; Laurent, G.; Pehau-Arnaudet, G.; Coelho, C.; Bonhomme-Coury, L.; Giraud-Guille, M.-M.; Babonneau, F.; Azaïs, T.; Nassif, N. Water-Mediated Structuring of Bone Apatite. *Nat. Mater.* **2013**, *12* (12), 1144−1153.
(35) Laurencin, D.; Gervais, C.; Wong, A.; Coelho, C.; Mauri, F.; Massiot, D.; Smith, M. E.; Bonhomme, C. Implementation of High Resolution 43Ca Solid State NMR Spectroscopy: Toward the Elucidation of Calcium Sites in Biological Materials. *J. Am. Chem. Soc.* **2009**, *131* (37), 13430−13440.
(36) Lee, D.; Leroy, C.; Crevant, C.; Bonhomme-Coury, L.; Babonneau, F.; Laurencin, D.; Bonhomme, C.; De Paëpe, G. Interfacial Ca 2+ Environments in Nanocrystalline Apatites Revealed by Dynamic Nuclear Polarization Enhanced 43 Ca NMR Spectroscopy. *Nat. Commun.* **2017**, *8* (1), No. 14104.
(37) Hu, K.-N.; Yu, H.; Swager, T. M.; Griffin, R. G. Dynamic Nuclear Polarization with Biradicals. *J. Am. Chem. Soc.* **2004**, *126* (35), 10844−10845.
(38) Ni, Q. Z.; Daviso, E.; Can, T. V.; Markhasin, E.; Jawla, S. K.; Swager, T. M.; Temkin, R. J.; Herzfeld, J.; Griffin, R. G. High Frequency Dynamic Nuclear Polarization. *Acc. Chem. Res.* **2013**, *46* (9), 1933−1941.
(39) Rossini, A. J.; Zagdoun, A.; Lelli, M.; Lesage, A.; Copéret, C.; Emsley, L. Dynamic Nuclear Polarization Surface Enhanced NMR Spectroscopy. *Acc. Chem. Res.* **2013**, *46* (9), 1942−1951.
(40) Lesage, A.; Lelli, M.; Gajan, D.; Caporini, M. A.; Vitzthum, V.; Miéville, P.; Alauzun, J.; Roussey, A.; Thieuleux, C.; Mehdi, A.; Bodenhausen, G.; Coperet, C.; Emsley, L. Surface Enhanced NMR Spectroscopy by Dynamic Nuclear Polarization. *J. Am. Chem. Soc.* **2010**, *132* (44), 15459−15461.
(41) Sauvée, C.; Rosay, M.; Casano, G.; Aussenac, F.; Weber, R. T.; Ouari, O.; Tordo, P. Highly Efficient, Water-Soluble Polarizing Agents for Dynamic Nuclear Polarization at High Frequency. *Angew. Chem., Int. Ed.* **2013**, *52* (41), 10858−10861.
(42) Vega, A. J. CPMAS of Quadrupolar S = 32 Nuclei. *Solid State Nucl. Magn. Reson.* **1992**, *1* (1), 17−32.
(43) Ashbrook, S. E.; Wimperis, S. Spin-Locking of Half-Integer Quadrupolar Nuclei in Nuclear Magnetic Resonance of Solids: Second-Order Quadrupolar and Resonance Offset Effects. *J. Chem. Phys.* **2009**, *131* (19), No. 194509.
(44) Amoureux, J.-P.; Pruski, M. Theoretical and Experimental Assessment of Single- and Multiple-Quantum Cross-Polarization in Solid State NMR. *Mol. Phys.* **2002**, *100* (10), 1595−1613.
(45) Barrie, P. J. Distorted Powder Lineshapes in 27 Al CP/MAS NMR Spectroscopy of Solids. *Chem. Phys. Lett.* **1993**, *208* (5), 486−490.
(46) Vitzthum, V.; Miéville, P.; Carnevale, D.; Caporini, M. A.; Gajan, D.; Copéret, C.; Lelli, M.; Zagdoun, A.; Rossini, A. J.; Lesage, A.; Emsley, L.; Bodenhausen, G. Dynamic Nuclear Polarization of Quadrupolar Nuclei Using Cross Polarization from Protons: Surface-Enhanced Aluminium-27 NMR. *Chem. Commun.* **2012**, *48* (14), 1988−1990.
(47) Blanc, F.; Sperrin, L.; Jefferson, D. A.; Pawsey, S.; Rosay, M.; Grey, C. P. Dynamic Nuclear Polarization Enhanced Natural Abundance 17O Spectroscopy. *J. Am. Chem. Soc.* **2013**, *135* (8), 2975−2978.
(48) Nagashima, H.; Trébosc, J.; Kon, Y.; Lafon, O.; Amoureux, J.-P. Efficient Transfer of DNP-Enhanced 1 H Magnetization to Half-Integer Quadrupolar Nuclei in Solids at Moderate Spinning Rate. *Magn. Reson. Chem.* **2021**, *59* (9−10), 920−939.
(49) Vioglio, P. C.; Thureau, P.; Juramy, M.; Ziarelli, F.; Viel, S.; Williams, P. A.; Hughes, C. E.; Harris, K. D. M.; Mollica, G. A Strategy for Probing the Evolution of Crystallization Processes by Low-Temperature Solid-State NMR and Dynamic Nuclear Polarization. *J. Phys. Chem. Lett.* **2019**, *10* (7), 1505−1510.
(50) Siegel, R.; Nakashima, T. T.; Wasylishen, R. E. Signal Enhancement of NMR Spectra of Half-Integer Quadrupolar Nuclei in Solids Using Hyperbolic Secant Pulses. *Chem. Phys. Lett.* **2004**, *388* (4), 441−445.
(51) Laurencin, D.; Wong, A.; Hanna, J. V.; Dupree, R.; Smith, M. E. A High-Resolution 43Ca Solid-State NMR Study of the Calcium Sites of Hydroxyapatite. *J. Am. Chem. Soc.* **2008**, *130* (8), 2412−2413.
(52) Massiot, D.; Fayon, F.; Capron, M.; King, I.; Le Calvé, S.; Alonso, B.; Durand, J.-O.; Bujoli, B.; Gan, Z.; Hoatson, G. Modelling One- and Two-Dimensional Solid-State NMR Spectra. *Magn. Reson. Chem.* **2002**, *40* (1), 70−76.
(53) van Meerten, S. G. J.; Franssen, W. M. J.; Kentgens, A. P. M. SsNake: A Cross-Platform Open-Source NMR Data Processing and Fitting Application. *J. Magn. Reson.* **2019**, *301*, 56−66.
(54) Kresse, G.; Hafner, J. Ab Initio Molecular-Dynamics Simulation of the Liquid-Metal–Amorphous-Semiconductor Transition in Germanium. *Phys. Rev. B* **1994**, *49* (20), 14251−14269.
(55) Giannozzi, P.; Baroni, S.; Bonini, N.; Calandra, M.; Car, R.; Cavazzoni, C.; Ceresoli, D.; Chiarotti, G. L.; Cococcioni, M.; Dabo, I.; Corso, A. D.; de Gironcoli, S.; Fabris, S.; Fratesi, G.; Gebauer, R.; Gerstmann, U.; Gougoussis, C.; Kokalj, A.; Lazzeri, M.; Martin-Samos, L.; Marzari, N.; Mauri, F.; Mazzarello, R.; Paolini, S.; Pasquarello, A.; Paulatto, L.; Sbraccia, C.; Scandolo, S.; Sclauzero, G.; Seitsonen, A. P.; Smogunov, A.; Umari, P.; Wentzcovitch, R. M. QUANTUM ESPRESSO: A Modular and Open-Source Software Project for Quantum Simulations of Materials. *J. Phys.: Condens. Matter* **2009**, *21* (39), No. 395502.
(56) Troullier, N.; Martins, J. L. Efficient Pseudopotentials for Plane-Wave Calculations. *Phys. Rev. B* **1991**, *43* (3), 1993−2006.
(57) Kleinman, L.; Bylander, D. M. Efficacious Form for Model Pseudopotentials. *Phys. Rev. Lett.* **1982**, *48* (20), 1425−1428.
(58) Pyykkö, P. Year-2017 Nuclear Quadrupole Moments. *Mol. Phys.* **2018**, *116* (10), 1328−1338.
(59) Perras, F. A.; Viger-Gravel, J.; Burgess, K. M. N.; Bryce, D. L. Signal Enhancement in Solid-State NMR of Quadrupolar Nuclei. *Solid State Nucl. Magn. Reson.* **2013**, *51*−*52*, 1−15.
(60) Schwarzenbach, G.; Ackermann, H. Komplexone V. Die Äthylendiamin-Tetraessigsäure. *Helv. Chim. Acta* **1947**, *30* (6), 1798−1804.
(61) Griko, Y. V. Energetics of Ca2+−EDTA Interactions: Calorimetric Study. *Biophys. Chem.* **1999**, *79* (2), 117−127.
(62) Iwahara, J.; Anderson, D. E.; Murphy, E. C.; Clore, G. M. EDTA-Derivatized Deoxythymidine as a Tool for Rapid Determination of Protein Binding Polarity to DNA by Intermolecular Paramagnetic Relaxation Enhancement. *J. Am. Chem. Soc.* **2003**, *125* (22), 6634−6635.
(63) Burgess, K. M. N.; Xu, Y.; Leclerc, M. C.; Bryce, D. L. Alkaline-Earth Metal Carboxylates Characterized by 43Ca and 87Sr Solid-State NMR: Impact of Metal-Amine Bonding. *Inorg. Chem.* **2014**, *53* (1), 552−561.
(64) Ramnarain, V.; Georges, T.; Peña, N. O.; Ihiawakrim, D.; Longuinho, M.; Bulou, H.; Gervais, C.; Sanchez, C.; Azaïs, T.; Ersen, O. Monitoring of CaCO3 Nanoscale Structuration through Real-Time Liquid Phase Transmission Electron Microscopy and Hyperpolarized NMR. *J. Am. Chem. Soc.* **2022**, *144* (33), 15236−15251.
(65) Miyatou, T.; Araya, T.; Ohashi, R.; Ida, T.; Mizuno, M. Hydration Water Dynamics in Bovine Serum Albumin at Low Temperatures as Studied by Deuterium Solid-State NMR. *J. Mol. Struct.* **2016**, *1121*, 80−85.
(66) Klug, D. D.; Mishima, O.; Whalley, E. High-density Amorphous Ice. IV. Raman Spectrum of the Uncoupled O−H and O−D Oscillators. *J. Chem. Phys.* **1987**, *86* (10), 5323−5328.

https://doi.org/10.1021/acsomega.3c08292
ACS Omega 2024, 9, 4881−4891

(67) Shalit, A.; Perakis, F.; Hamm, P. Disorder-Suppressed Vibrational Relaxation in Vapor-Deposited High-Density Amorphous Ice. *J. Chem. Phys.* **2014**, *140* (15), No. 151102.
(68) Laurencin, D.; Wong, A.; Dupree, R.; Smith, M. E. Natural Abundance 43Ca Solid-State NMR Characterisation of Hydroxyapatite: Identification of the Two Calcium Sites. *Magn. Reson. Chem.* **2008**, *46* (4), 347−350.

https://doi.org/10.1021/acsomega.3c08292
ACS Omega 2024, 9, 4881−4891